# Deep Learning Based Near-Field Positioning in True-Time-Delay Array Systems

Roman Klus*†, Jukka Talvitie*, Ibrahim Pehlivan†, Mehmet C. Ilter*, Lucie Klus*†, Danijela Cabric†, and Mikko Valkama*
*Tampere University, Tampere, Finland; †University of California, Los Angeles, USA

***Abstract*—In millimeter-wave (mmW) networks, large antenna arrays can be deployed to combat high signal attenuation, yet creating also near-field (NF) effects in the relative proximity of the antenna system. While utilizing frequency-selective rainbow beams enabled by true-time-delay (TTD) analog beamformer, we study the mmW network localization capabilities in the NF domain via deep learning neural networks. By leveraging the unique properties of the rainbow beams, we show that the proposed deep learning model, referred to as RaiNet, is capable of accurately positioning the user using a single channel response measurement. The provided numerical results at different carrier frequencies show that the proposed deep learning approach enables significant improvements in localization accuracy, compared to the state-of-the-art benchmark methods. The study thus paves the way for advanced localization techniques in 6G systems, contributing to the development of more efficient and intelligent future networks.**

***Index Terms*—Analog Beamforming, Deep Learning, Localization, mmWaves, Near-field, Positioning, Rainbow Beams, TTD**

## I. Introduction

In millimeter-wave (mmW) networks, large antenna arrays are commonly considered, enabling highly efficient spatial multiplexing and other beamforming capabilities, while facilitating also sensing and localization [1]. On the other hand, with large apertures, the user equipment (UE) may also be located within the near-field (NF) domain, and traditional beamforming techniques applicable in far-field (FF) systems become ineffective [2]. To this end, by utilizing the true-time-delay (TTD) elements along with radio frequency (RF) phase shifts (PSs), new functionalities are enabled, increasing the flexibility of the analog beamformer [3]. In this work, we consider a TTD-based mmW antenna array connected to a single analog RF chain, and specifically focus on the UE localization challenge for varying UE distances and directions within the NF domain. The considered scenario is illustrated in Fig. 1 where the network gNodeB (gNB) observes the uplink (UL) reference signal transmissions through the so-called rainbow beams (RBs) [4], forming the physical basis for localization.

The concept of RBs was originally proposed in [4] for the sake of accelerated beam training in the FF region, exploiting the inherent beam-split effect. By controlling the RBs using the TTD elements, beams at different frequencies can flexibly occupy *different locations in space*. In [5], the authors extend the RBs for beam training in NF as well. In [6], the authors proposed to virtually split a single analog antenna array into 3 virtual sub-arrays, and used orthogonal matching pursuit (OMP) to decompose a single NF channel measurement into FF ones, enabling triangulation-based beam training.

This work was supported by the Research Council of Finland under the grants #352754, #357730, and #359095. This material is also based upon work supported by the National Science Foundation under Grant No. 2224322. L. Klus acknowledges funding from Nokia Foundation, grant number 20240403.

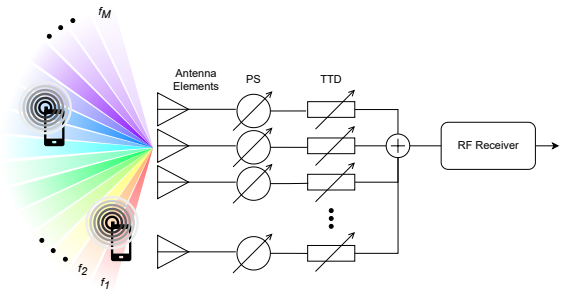


Fig. 1. Considered uplink system model, where omnidirectional UE transmission is observed by the gNB through the so-called rainbow beams, enabled by a TTD array.

NF localization scheme in mmW TTD system context was proposed in [7], considering a hybrid sub-array architecture while utilizing OMP with triangulation. The authors of [8], in turn, propose the utilization of RBs in a radar system while exploiting the Doppler frequencies of each user. Exploiting the beam-squint effect for localization was also considered in [9], which relies on channel power response measurement but requires multiple pilot symbols while separately estimating the distance and angle. The prior deep learning-based positioning model proposed in [10] relies on the initial estimate from [9], followed by a rather complex convolutional architecture.

In this work, building on the idea of utilizing FF RBs with an analog beamformer in [6], we exploit the characteristics of the beamformed radio channel in NF for UE localization using a single uplink reference symbol. Such an approach has not been reported earlier in the existing literature, as all the related works in [7]–[10] consider either multiple RF chains or multiple pilot symbols. Moreover, the proposed solution improves the resilience to noise within the channel by exploiting the channel amplitude response, rather than relying on the received signal phase. The main technical contributions and novelty of the work can be summarized as follows:

- We introduce the FF rainbow-beam-based beamformer and characterize its behaviour in the NF region, providing visualization and rationale behind its utilization for localization.
- We propose a low-complexity, yet effective artificial neural network (ANN) architecture denoted as Rainbow

beam Network (RaiNet), capable of highly accurate user localization in the NF region.
- We evaluate the proposed model at different carrier frequencies while also varying the UE transmit power to demonstrate the applicability of rainbow beams for localization in NF, and assess the proposed RaiNet's capabilities against relevant benchmarks.

## II. Fundamentals and System Model

### A. Localization in mmW Networks

The elementary task of the localization model in wireless networks is to estimate the position of the user in the given coordinate system while utilizing the information within the received signal [1]. The localization algorithms are generally split into model-based and data-based solutions. Model-based solutions rely on the known coordinates of the receiver (RX) and its antenna elements, known channel behaviour, and rely on the specific mathematical model. Data-driven methods, such as machine learning (ML) approaches or $k$-Nearest Neighbors ($k$-NN), rely on a model that was trained using a pre-existing database of labeled samples. In its simplest form, the localization model can be expressed as a function $\hat{\mathbf{l}} = F(\mathbf{f})$, where $\mathbf{f}$ denotes a vector of features, $\hat{\mathbf{l}} = [\hat{x}, \hat{y}]$ a vector of estimated locations, and $F(\cdot)$ denotes the model itself.

Within current wireless networks, measured received signal strength (RSS) is utilized across network functions and is one of the most common features used for positioning [11]. The fifth generation (5G) New Radio (NR) standard distinguishes several RSS-based metrics, while considering beam-specific quantities [12]. Nevertheless, despite being highly computationally efficient, capturing the entire channel using a single number removes the majority of the information from the measurements. For increased reliability as well as enabling numerous network functionalities, utilizing the channel response becomes necessary, especially at the mmW bands [13].

### B. Near-Field Channel with Analog TTD Beamformer

As high-frequency signals suffer from severe attenuation due to scattering and diffraction, the mmW communication systems assume the availability of the line-of-sight (LoS) link [14]. Consequently, this work focuses on the LoS channel scenario, although similar positioning performance in the non-line-of-sight (NLoS) region is achievable when considering the ML-based models [13]. The scenario studied in this work considers an UL transmission from a UE equipped with a single antenna towards the gNB equipped with uniform linear array (ULA) with $N$ antenna elements. Furthermore, the given bandwidth $B$ around a carrier frequency $f_c$ is divided into $M$ subcarriers with subcarrier spacing (SCS) of $\Delta f = \frac{B}{M}$. The UE is located in the NF region, i.e., within the Rayleigh distance from the transmitter [15].

*1) Near-Field Channel Model:* The received signal $\mathbf{y}^{(n)}$ at each antenna element $n = 1, ..., N$ of the ULA is expressed as $\mathbf{y}^{(n)} = \mathbf{h}^{(n)}\mathbf{x} + \boldsymbol{\epsilon}^{(n)}$, where $\mathbf{x}$ denotes the transmitted signal and $\boldsymbol{\epsilon}^{(n)}$ is the signal uncertainty considered as additive white Gaussian noise (AWGN). Furthermore, a flat-fading channel with free-space path-loss (PL) is considered, which can be characterized as [5]

$$h_m^{(n)} = \frac{\lambda_m}{4\pi r^{(n)}} e^{-jk_m r_0^{(n)}}, \tag{1}$$

where $k_m = 2\pi f_m / c$ is the wave number at the given subcarrier frequency, $c$ is the speed of light in vacuum, $r^{(n)}$ is the physical distance between the UE and the $n^{th}$ antenna element, and $\lambda_m = \frac{f_m}{c}$ is the wavelength corresponding to the $m^{th}$ subcarrier. Finally, $f_m$ is the $m^{th}$ subcarrier frequency, which can be expressed as

$$f_m = f_c + \Delta f(m - \frac{M+1}{2}). \tag{2}$$

*2) Analog Far-Field Rainbow:* The individual antenna elements at the gNB are each equipped with tunable PSs and TTDs, followed by a combiner and a single RF chain processing the received signal. In order to create the RBs at the beamformer, the phase rotations $\phi_n$ and delays $\tau_n$ at TTD are configured so that

$$\phi_n = \frac{2\pi f_c}{B}(n - \frac{N+1}{2}), \tag{3}$$

and

$$\tau_n = \frac{1}{B}(n - \frac{N+1}{2}), \tag{4}$$

following the approach proposed in [6]. We note that (3) and (4) correspond to the FF rainbow beam patterns despite focusing on localizing the user in the NF region. As the delay in the time domain corresponds to frequency-dependent phase shifts in the frequency domain, the delay elements create varying antenna-specific phase shifts in the received signal frequency content, and consequently create a beamformed pattern across the spectrum in both spatial and frequency domains.

## III. Proposed Localization Method

Before introducing the details on the utilized ANN model, it is important to understand the unique characteristics of the FF RB in the NF domain. This is highlighted and visualized through a concrete example in the below Section III.A, followed then by the actual localization approach and the RaiNet ANN model in Sections III.B and III.C.

### A. Understanding the FF RB Channel in the NF Region

The considered example scenario is depicted in Fig. 2a, visualizing the UE situated at three example distances and angles from the ULA, each corresponding to different channel power responses presented in Fig. 2b. The considered exact parametrization can be found later in Section IV-A. Due to utilizing the FF RBs at the gNB, the RX observes the UE at the limited sub-band, i.e. set of subcarriers, determined by both the distance and the angle at which the transmitter (TX) (here UE) is located. Fig. 2b shows that the frequency domain channel power response after RB (later referred to as channel) of the first (red) user, situated 60 m from the ULA at 30° angle, is significantly narrower and observed at lower-frequency subcarriers than that of the second (green) user, situated at 10 m and 0° from the ULA. The third (blue) user's channel is showing a further increased

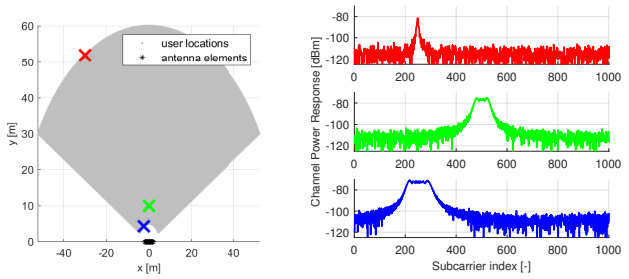


(a) (b)

Fig. 2. (a) Visualization of the considered deployment with 3 example UEs located in the NF region and (b) their corresponding channel power responses after TTD-based RBs.

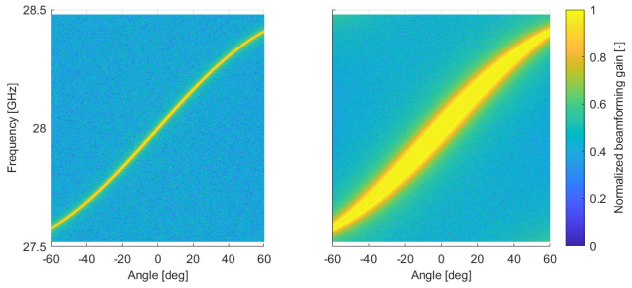


(a) (b)

Fig. 3. Normalized beamforming gain of the rainbow-beam beamformer in the angle-frequency domain for UE located at (a) 60 m and (b) 5 m distance from the ULA. The data correspond to $f_c = 28$ GHz.

observable bandwidth, as he is situated at 5 m and 30° from the ULA, i.e. at a lower distance.

It can easily be observed that the channel after the FF RB in the NF region is characterized by the active sub-band, which varies in width based on the distance between the TX and the RX. To further highlight the channel behavior, Fig. 3a depicts the normalized RB beamforming gain in the angle-frequency domain at 60 m from the antenna, while Fig. 3b shows the corresponding behaviour at 5 m. The continuous shift in the width of the channel is visible when moving through the NF region towards Rayleigh distance, while the indices of the observable subcarriers change based on the angle between the ULA and the UE. Furthermore, Fig. 3a and Fig. 3b show that rather than deploying a discrete number of beams, the FF RB approach creates a continuous spectrum across angles and frequencies, enabling efficient sensing capabilities. The nonlinear angle-to-subcarrier mapping visible in the figures is a characteristic inherited from the RB definition, with higher angular resolution at the boresight.

### B. Localization Through Beamformed Responses

Based on the above formulation and visualization of the FF RBs in the NF region, we can establish the following. Firstly, the width of the active sub-band corresponding to each user depends on that user's distance from the gNB. Secondly, the indices of the active subcarriers of each user depend on that user's angular orientation with respect to the gNB. Consequently, frequency responses after FF RB in the NF region show clear *location-specific patterns* and can be exploited at the gNB to localize the UE using a data-driven approach. Moreover, we claim and demonstrate that robust models, such as ANNs can achieve this using only a single reference symbol during the initial access phase, effectively accelerating the establishment of the beamformed radio link to the corresponding user(s).

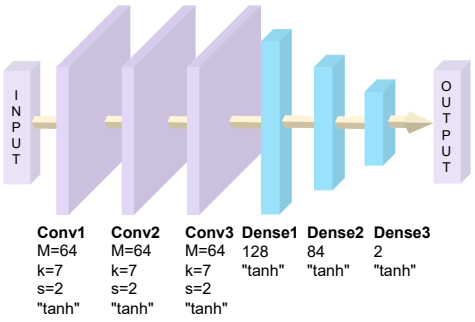


Fig. 4. The structure and hyperparameters of the proposed RaiNet model.

For clarity, we highlight that the utilization of RBs significantly reduces the number of observable subcarriers at the gNB despite the UE transmitting at the entire bandwidth, as shown in Fig. 2b. Consequently, utilizing RBs is not directly suitable for the actual payload data communications. Despite that, their effectiveness as a sensing approach can be exploited for lightweight and reliable localization.

### C. RaiNet Model Architecture

The actual localization model proposed in this work is an ANN regression model harnessing the LeNET architecture [16], which combines convolutional and densely connected layers to enable inference on data with strong uncertainties while sustaining low computational and architectural complexity. The outline of the RaiNet model is shown in Fig. 4, including the hyperparameters of each layer. In each realization, the model was trained for 50 epochs using approximately 250 000 noisy samples.

The proposed architecture can effectively capture the varying outline of the RB channel within the convolutional layers and transform the extracted features into a location estimate in the fully connected part. The model considers a single realization of an amplitude response as an input feature $\mathbf{f}$ acquired in a single pilot measurement of the noisy channel. The phase of the signal is often highly distorted in less favorable signal-to-noise ratio (SNR) scenarios, while processing complex-valued quantities requires increasing the parameter count of the ANN model, adding to its complexity. Moreover, complementary experimental evaluations showed that removing the phase does not decrease the achieved positioning performance. Finally, RaiNet considers true user locations in the Cartesian coordinate system as labels.

## IV. Numerical Results

### A. Evaluation Scenario and Assumptions

An overview of the considered physical system parameters is provided in Table I, including the number of antennas $M$, the number of subcarriers $N$, and the antenna spacing $A_{spac.}$. We consider physical thermal noise power, $P_n$, directly calculated through the bandwidth $B$ at an example temperature of 300 K,

TABLE I: CONSIDERED PHYSICAL SYSTEM PARAMETERS

| $M$ [antennas] | $N$ [subcarriers] | $A_{spac.}$ [m] | $P_{Tx}$ [dBm] | $P_n$ [dBm] |
|---|---|---|---|---|
| 255 | 1001 | $\lambda/2$ | +23 | –84 |

TABLE II: DATA PROPERTIES AT DIFFERENT CARRIER FREQUENCIES

| $f_c$ [GHz] | $\Delta f$ [kHz] | $B$ [GHz] | $A_{spac.}$ [mm] | $A_{size}$ [m] | $\mathcal{R}_{dist}$ [m] | $\mathcal{F}_{dist}$ [m] |
|---|---|---|---|---|---|---|
| 28 | 240 | 0.24 | 5.4 | 1.36 | 345.4 | 7.66 |
| 60 | 960 | 0.961 | 2.5 | 0.635 | 161.2 | 3.58 |
| 100 | 960 | 0.961 | 1.5 | 0.381 | 96.7 | 2.1 |

while change the radiated power $P_{Tx}$ to control the radio link quality, i.e., the SNR.

Furthermore, we consider three distinct carrier frequencies, as noted in Table II, to show the general applicability of the solution. We further list the specific subcarrier spacing $\Delta f$, bandwidth $B$, antenna spacing $A_{spac.}$, and antenna size $A_{size}$, as well as Rayleigh distance $\mathcal{R}_{dist}$ and Fresnel distance $\mathcal{F}_{dist}$, which characterize the NF [15]. The selected numerologies are consistent with those proposed for the emerging networks [17].

The evaluation scenario of interest follows the visualization shown in Fig. 2a, with the UE situated at 5 to 60 meters distance in front of the ULA, at angles between $-60°$ and $60°$, ensuring narrow beam patterns in the NF [4]. The common evaluation dataset, shared across all models, considers a grid of UE coordinates spaced $0.5\,\text{m}$ in range and $0.5°$ in angle. A separate evaluation dataset was created for each considered carrier frequency $f_c$ and each of the three transmit powers of the UE, namely $+23$, $+13$, and $+3\,\text{dBm}$.

### B. Benchmark Models

The first considered baseline is $k$-NN, a simple yet powerful matching algorithm that in many cases outperforms recent ANN models [18]. The first parametrization, denoted 1-NN, corresponds to Euclidean distance and $k = 1$, representing a naive classification algorithm and essentially equates to a maximum likelihood solution. The second setup, W-11-NN, includes Euclidean distance with linear weighting and number of considered neighbors $k = 11$, which was found experimentally as the best-performing setup. The model considers the same features as the proposed model, while the codebook, i.e. the testing dataset, was generated as $10\,000$ randomly sampled noise-free channel measurements.

The second baseline is the virtual sub-array sparse rainbow (VSSR) algorithm, which is a fast NF beam-training algorithm [6], that utilizes rainbow TTD beams and virtually partitions the array into 3 sub-arrays such that a user who is in NF for the entire array falls into FF for each sub-array. Then, the VSSR algorithm recovers each sub-array's signal using OMP, determines the signal angle-of-arrival (AoA) for each sub-array, and triangulates the user location from known array geometry. The algorithm utilizes a dictionary with $10\,010$ possible angles for each sub-array.

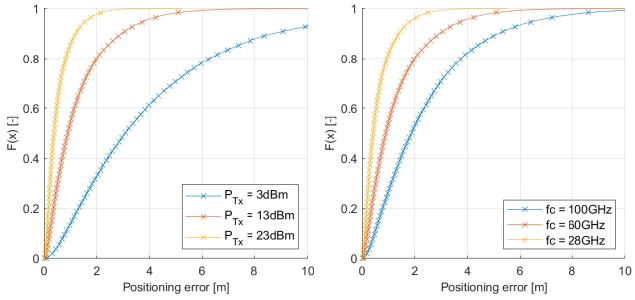


(a) (b)

Fig. 5. ECDFs of RaiNet-based localization errors (a) for varying transmit powers $P_{Tx}$ at $f_c = 60$ GHz and (b) for varying carrier frequencies $f_c$ at $P_{Tx} = +13$ dBm.

### C. Empirical Results and Findings

In the paragraphs below, we provide a numerical evaluation of the proposed model and the impact of the NF effect, as well as discuss the conclusions these results offer. The precise numerical values are to be found in Table III, listing mean positioning error $\mu$, where the positioning errors were computed as $\|l - \hat{l}\|$, $90^{\text{th}}$ percentile error $p_{90}$, mean ranging error $\mu_\rho$, and mean angular error $\mu_\theta$.

The numerical results show that in terms of *localization accuracy*, RaiNet performs the best at all carrier frequencies and transmit powers, reaching $0.28\,\text{m}$ mean positioning error at $f_c = 28\,\text{GHz}$. In terms of *angle-estimation accuracy*, the proposed model is outperformed by the $k$-NN baselines, which perform close-to-perfectly, reliably finding the match in the active subcarriers, while poorly estimating the *range*. We note that the proposed model was trained with labels in the Cartesian system and thus, the angle-estimation capabilities were not directly included in the objective function. The performance of the VSSR baseline, in turn, changes based on the carrier frequency more significantly than that of the remaining models; while at 28 GHz and $P_{Tx} = +23\,\text{dBm}$ achieves sub-meter localization accuracy, competitive with RaiNet, it is strongly outperformed at higher-frequencies by the proposed method.

Fig. 5a presents the empirical cumulative distribution functions (ECDFs) of the positioning performance of varying $P_{Tx}$ corresponding to the RaiNet model's estimates, showing consistent results without significant outliers. The decrease in performance at lower transmit powers $P_{Tx}$ corresponds to the poorer SNR. Similarly, Fig. 5b depicts the ECDFs of the positioning performance while varying the carrier frequency $f_c$. The decrease in performance at higher carrier frequencies $f_c$ corresponds to the higher PL, as well as to the reduced NF effect due to the smaller antenna aperture (ULA size is set to 255 antenna elements with $\lambda/2$ spacing).

We further visualize the distribution of errors in the spatial domain, shown in Fig. 6a–6d. The localization accuracy across models deteriorates when moving further from the gNB, with only the RaiNet model sustaining its positioning capabilities at further distances, having only individual poorly localized samples. W-11-NN model's localization capabilities start consistently deteriorating at distances of $50\,\text{m}$ (Fig 6c), while the 1-NN model's limit reached $30\,\text{m}$ (Fig 6b). The errors

TABLE III: SUMMARY OF NUMERICAL RESULTS INCLUDING THE PROPOSED RAINET APPROACH AND THREE BENCHMARK METHODS

| | | RaiNet (proposed) | | | | 1-NN | | | | W-11-NN | | | | VSSR [6] | | | |
|---|---|---|---|---|---|---|---|---|---|---|---|---|---|---|---|---|---|
| $f_c$ [GHz] | $P_{Tx}$ [dBm] | $\mu$ [m] | $p_{90}$ [m] | $\mu_\rho$ [m] | $\mu_\theta$ [rad] | $\mu$ [m] | $p_{90}$ [m] | $\mu_\rho$ [m] | $\mu_\theta$ [rad] | $\mu$ [m] | $p_{90}$ [m] | $\mu_\rho$ [m] | $\mu_\theta$ [rad] | $\mu$ [m] | $p_{90}$ [m] | $\mu_\rho$ [m] | $\mu_\theta$ [rad] |
| 28 | +3 | 1.82 | 4.06 | 1.76 | 0.01 | 4.87 | 12.01 | 4.87 | 0.00 | 3.91 | 10.28 | 3.91 | 0.00 | 3.36 | 8.94 | 3.34 | 0.00 |
| 28 | +13 | 0.61 | 1.39 | 0.58 | 0.00 | 1.82 | 4.36 | 1.82 | 0.00 | 1.83 | 4.65 | 1.83 | 0.00 | 1.04 | 2.87 | 1.04 | 0.00 |
| 28 | +23 | 0.28 | 0.56 | 0.26 | 0.00 | 1.57 | 3.64 | 1.57 | 0.00 | 1.87 | 4.33 | 1.87 | 0.00 | 0.36 | 0.99 | 0.36 | 0.00 |
| 60 | +3 | 4.34 | 8.66 | 3.62 | 0.04 | 10.84 | 24.43 | 10.75 | 0.00 | 9.39 | 22.49 | 9.31 | 0.00 | 16.34 | 52.66 | 14.78 | 0.23 |
| 60 | +13 | 1.28 | 2.92 | 1.24 | 0.01 | 3.42 | 8.41 | 3.42 | 0.00 | 2.75 | 7.04 | 2.75 | 0.00 | 4.92 | 12.78 | 4.81 | 0.01 |
| 60 | +23 | 0.53 | 1.19 | 0.50 | 0.00 | 2.09 | 4.80 | 2.09 | 0.00 | 2.84 | 6.18 | 2.84 | 0.00 | 1.53 | 4.21 | 1.53 | 0.00 |
| 100 | +3 | 13.32 | 31.39 | 7.67 | 0.22 | 17.36 | 38.14 | 16.00 | 0.00 | 16.25 | 37.48 | 14.99 | 0.00 | 25.73 | 55.11 | 22.67 | 0.78 |
| 100 | +13 | 2.43 | 5.15 | 2.32 | 0.01 | 5.67 | 13.56 | 5.67 | 0.00 | 4.10 | 10.38 | 4.10 | 0.00 | 10.81 | 28.85 | 9.05 | 0.10 |
| 100 | +23 | 0.79 | 1.77 | 0.76 | 0.00 | 2.51 | 5.73 | 2.51 | 0.00 | 3.37 | 6.90 | 3.37 | 0.00 | 3.41 | 9.50 | 3.34 | 0.00 |

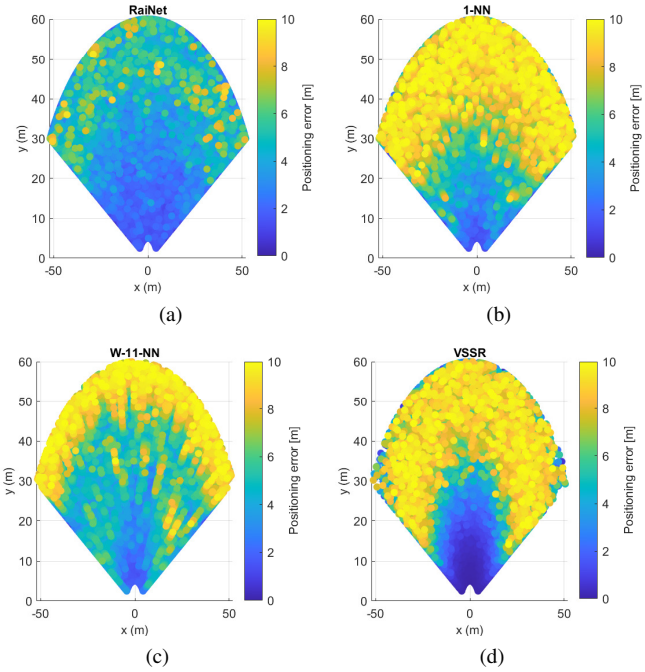


Fig. 6. Visualization of positioning errors for (a) RaiNet (proposed), (b) 1-NN, (c) W-11-NN, and (d) VSSR at $P_{Tx} = 13$ dBm and $f_c = 60$ GHz.

of the VSSR algorithm show that in the immediate proximity to the gNB, the algorithm performs close to perfectly, as indicated by dark blue color in Fig 6d, while clearly deteriorating above a certain distance. Such behavior can be attributed to the VSSR strongly depending on actual SNR, NF effect, as well as not utilizing the received signal power in the process. The other model-based solutions, such as maximum likelihood, are in theory capable of approaching the Cramér–Rao bound in high SNR regimes, but fall short when the signal characteristics start approaching FF behaviour.

## V. CONCLUSION

This work introduced an effective approach of utilizing FF rainbow beams for ANN-based localization in the NF region of extremely large analog TTD arrays, while requiring only a single uplink reference symbol. The work highlighted and characterized the rainbow beams' behavior and the corresponding connection to location information in the NF region – and proposed RaiNet, a low-complexity, yet powerful localization model, combining convolutional and fully connected neural processing layers. Via numerical evaluations at different mmW bands, RaiNet was shown to clearly outperform the prior-art benchmark solutions. Our future work will focus on extending the study to tracking capabilities, as well as considering multipath propagation.

## REFERENCES


[1] N. González-Prelcic *et al.*, "The Integrated Sensing and Communication Revolution for 6G: Vision, Techniques, and Applications," *Proceedings of the IEEE*, vol. 112, no. 7, pp. 676–723, 2024.

[2] A. M. Elbir *et al.*, "Near-field Signal Processing: Unleashing the Power of Proximity," *IEEE Signal Process. Magazine*, vol. 42, pp. 20–32, 2025.

[3] C. Lin, G. Y. Li, and L. Wang, "Subarray-based Coordinated Beamforming Training for mmWave and sub-THz Communications," *IEEE J. on Sel. Areas in Commun.*, vol. 35, no. 9, pp. 2115–2126, 2017.

[4] H. Yan, V. Boljanovic, and D. Cabric, "Wideband Millimeter-wave Beam Training with True-time-delay Array Architecture," in *53rd Asilomar Conference on Signals, Syst., and Comput.* IEEE, 2019, pp. 1447–1452.

[5] M. Cui *et al.*, "Near-Field Rainbow: Wideband Beam Training for XL-MIMO," *IEEE Trans. on Wireless Commun.*, vol. 22, no. 6, pp. 3899–3912, 2022.

[6] I. Pehlivan *et al.*, "Near-Field Beam Training with Analog Extremely Large True-Time-Delay Arrays," in *2024 Conference Record of the Fifthy Eight Asilomar Conference on Signals, Systems and Computers*, 2024.

[7] Z. Lu *et al.*, "Near-Field Localization and Channel Reconstruction for ELAA Systems," *IEEE Trans. on Wireless Commun.*, vol. 23, no. 7, pp. 6938–6953, 2023.

[8] G. Zhou *et al.*, "Rainbow Beams for Wideband mmWave Radar: Beam Training," in *2024 IEEE Wireless Communications and Networking Conference (WCNC)*. IEEE, 2024, pp. 1–6.

[9] H. Luo *et al.*, "Beam Squint Assisted User Localization in Near-field Integrated Sensing and Communications Systems," *IEEE Transactions on Wireless Communications*, vol. 23, no. 5, pp. 4504–4517, 2023.

[10] H. Lei *et al.*, "Deep Learning-Based Near-Field User Localization With Beam Squint in Wideband XL-MIMO Systems," *IEEE Transactions on Wireless Communications*, vol. 24, no. 2, pp. 1568–1583, 2025.

[11] S. E. Trevlakis *et al.*, "Localization as a Key Enabler of 6G Wireless Systems: A Comprehensive Survey and an Outlook," *IEEE Open Journal of the Communications Society*, vol. 4, pp. 2733–2801, 2023.

[12] 3GPP, "Physical Layer Measurements," Technical Report (TR) 38.215, V16.4.0, Jan. 2021.

[13] R. Klus *et al.*, "Robust NLoS Localization in 5G mmWave Networks: Data-Based Methods and Performance," *IEEE Transactions on Vehicular Technology*, vol. 74, no. 1, pp. 1534–1550, 2025.

[14] R. Schroeder, J. He, and M. Juntti, "Near-Field Channel Estimation for Extremely-Large Single-RF-Chain RIS Systems," in *Proc. IEEE SPAWC*, 2024, pp. 266–270.

[15] M. Cui *et al.*, "Near-Field MIMO Communications for 6G: Fundamentals, Challenges, Potentials, and Future Directions," *IEEE Communications Magazine*, vol. 61, no. 1, pp. 40–46, 2022.

[16] Y. LeCun *et al.*, "Gradient-Based Learning Applied to Document Recognition," *Proc. IEEE*, vol. 86, no. 11, pp. 2278–2324, 1998.

[17] M. Sarajlić *et al.*, "Waveforms for sub-THz 6G: Design Guidelines," in *Proc. EuCNC/6G Summit*, 2023, pp. 168–173.

[18] L. Klus, E. S. Lohan, and M. Valkama, "Employing Signal Statistics for Universal Fingerprinting Solution," in *Proc. IEEE VTC-Fall*, 2024.